

Charge Density Wave Activated Excitons in TiSe_2 - MoSe_2 Heterostructures

Jaydeep Joshi,^{1,2} Benedikt Scharf,³ Igor Mazin,^{1,2} Sergiy Krylyuk,⁴ Daniel J. Campbell,⁵
Johnpierre Paglione,^{5,6} Albert Davydov,^{4,2,5} Igor Žutić,⁷ and Patrick M. Vora*^{1,2}

¹*Department of Physics and Astronomy, George Mason University, Fairfax,
Virginia 22030, United States*

²*Quantum Science and Engineering Center, George Mason University, Fairfax,
Virginia 22030, United States*

³*Institute for Theoretical Physics and Astrophysics and Würzburg-Dresden Cluster
of Excellence ct.qmats, University of Würzburg, Am Hubland, 97074, Würzburg,
Germany*

⁴*Materials Science and Engineering Division, National Institute
of Standards and Technology, Gaithersburg, Maryland 20899,
United States*

⁵*Maryland Quantum Materials Center, Department of Physics,
University of Maryland, College Park, Maryland 20742,
United States*

⁶*Canadian Institute for Advanced Research, Toronto, Ontario M5G 1Z8,
Canada*

⁷*Department of Physics, University at Buffalo, Buffalo, New York 14260,
United States*

Layered materials enable the assembly of a new class of heterostructures where lattice-matching is no longer a requirement. Interfaces in these heterostructures therefore become a fertile ground for unexplored physics as dissimilar phenomena can be coupled via proximity effects. In this article we identify an unexpected photoluminescence (PL) peak when MoSe₂ interacts with TiSe₂. A series of temperature-dependent and spatially-resolved PL measurements reveal this peak is unique to the TiSe₂ - MoSe₂ interface, higher in energy compared to the neutral exciton, and exhibits exciton-like characteristics. The feature disappears at the TiSe₂ charge density wave transition, suggesting that the density wave plays an important role in the formation of this new exciton. We present several plausible scenarios regarding the origin of this peak that individually capture some aspects of our observations, but cannot fully explain this feature. These results therefore represent a fresh challenge for the theoretical community and provide a fascinating way to engineer excitons through interactions with charge density waves.

I. INTRODUCTION

Two-dimensional (2D) material interfaces in van der Waals (vdW) heterostructures provide a fascinating playground to explore proximity effects.¹ The relaxation of lattice constraints on heterostructure assembly allows for the arbitrary stacking of 2D materials.² These interfaces may, in some cases, support emergent states absent from the parent compounds, with superconductivity in twisted bilayer graphene and moiré excitons in transition metal dichalcogenides (TMDs) serving as remarkable examples.^{3–6} Many studies of vdW heterostructures incorporate semiconducting TMDs as an active component. This commonality is due to the availability of high-quality samples, well-established exfoliation procedures,^{7,8} and the existence of tightly-bound 2D excitons.⁹

The zoology of excitons in monolayer (ML) semiconductors is vast: neutral (X^0) and charged excitons or trions (X^- or X^+),^{9–12} neutral and charged biexcitons^{13–16} and dark exciton states^{17–20} have all been observed and exhaustively studied in semiconducting TMDs. The 2D nature of TMD excitons also renders them highly sensitive to the local dielectric environment^{21–26} allowing for a remote, contact-free probe of interface characteristics in vdW heterostructures. For instance, semiconductor hetero-bilayer and homo-bilayer heterostructures exhibit new PL emission peaks from interlayer excitons and splitting of exciton peaks due to the moiré potential.^{5,27–30} Proximity effects between 2D magnets and semiconductors lead to large valley splittings,^{31,32} and magnetic manipulation of exciton PL energy, intensity, and selection rules.^{1,33–35} Exotic correlated insulating states such as Wigner crystals and Mott insulators in twisted TMD semiconductor heterostructures are also observable in PL spectra.^{36–38} However, there have been no studies exploring the impact of similar electron correlated phases such as charge density waves (CDWs) on PL in vdW heterostructures.

Here we investigate optical signatures of interlayer coupling between the semiconductor MoSe₂ and the putative excitonic insulator 1T-TiSe₂,^{39–43} which hosts a commensurate 2×2 CDW state below 200 K. We find that the CDW alters the manifold of optically-active excitons at the TiSe₂ - MoSe₂ interface, which results in a new PL peak above X^0 . This feature, referred to as H1, appears in the MoSe₂ PL spectrum with a linewidth comparable to X^0 . While lower-energy PL sidebands are relatively common in TMDs due to phonon replicas and exciton localization,^{44–48} these observations are the first such detection of a higher-energy PL sideband. Detailed temperature-, power-, and spatially-resolved PL mea-

measurements on multiple heterostructures demonstrate that H1 has an origin consistent with a native exciton state rather than a localized exciton or defect state. However, H1 disappears at the TiSe_2 CDW temperature which suggests these two phenomena are closely linked. We have identified multiple plausible scenarios and discuss them in detail, although none are able to explain all aspects of our observations. Interactions between excitons and CDWs provide a fresh challenge to the theoretical community and a novel method for engineering excitons in 2D materials.

II. RESULTS

A. Optical characterization of vdW heterostructures

Optical microscope images of two TiSe_2 - MoSe_2 vdW heterostructures termed Sample 1 and Sample 2, respectively, are presented in Figs. 1(a) and 1(b). These samples are assembled by a modified viscoelastic method⁴⁹ that incorporates atomic force microscope (AFM) cleaning.⁵⁰ The black dashed line outlines the ML- MoSe_2 flake in each sample. Representative low-temperature (5 K) PL spectra on (black) and off (red) the interface are shown in Figs. 1(c) and 1(d) for the two samples. Emission from the MoSe_2 X^- (≈ 1.62 eV) and X^0 (≈ 1.65 eV) states agrees with prior observations in both energy and linewidth.^{11,18,51-53} The interface PL spectra contains a previously unobserved feature, referred to as H1, at ≈ 1.68 eV. H1 is comparable to X^0 in both intensity and linewidth for Sample 1, while being weaker and broader in Sample 2.

The 5 K PL spectra also show evidence of an anti-correlation between H1 and X^- . Spatially resolved PL maps of the interface allow us to explore this behavior further and connect it to interface quality by examining the integrated intensity ratios X^-/X^0 (Figs. 1(e) and 1(f)) and $\text{H1}/X^0$ (Figs. 1(g) and 1(h)). H1 and $X^0 + X^-$ integrated intensities are plotted separately in Supporting Information Fig. S1. For Sample 1, the ratio of X^-/X^0 (Fig. 1(e)) varies between 1-2 over most of the MoSe_2 flake with a notable jump at the crack on the bottom left quadrant of the map. On the heterostructure itself, this ratio plummets to well below 1 indicating the absence of free charges that can participate in trion formation. The connection of the X^-/X^0 ratio to charge transfer is well established in numerous reports^{11-13,54} and, since the transfer efficiency is exponentially dependent on distance, can

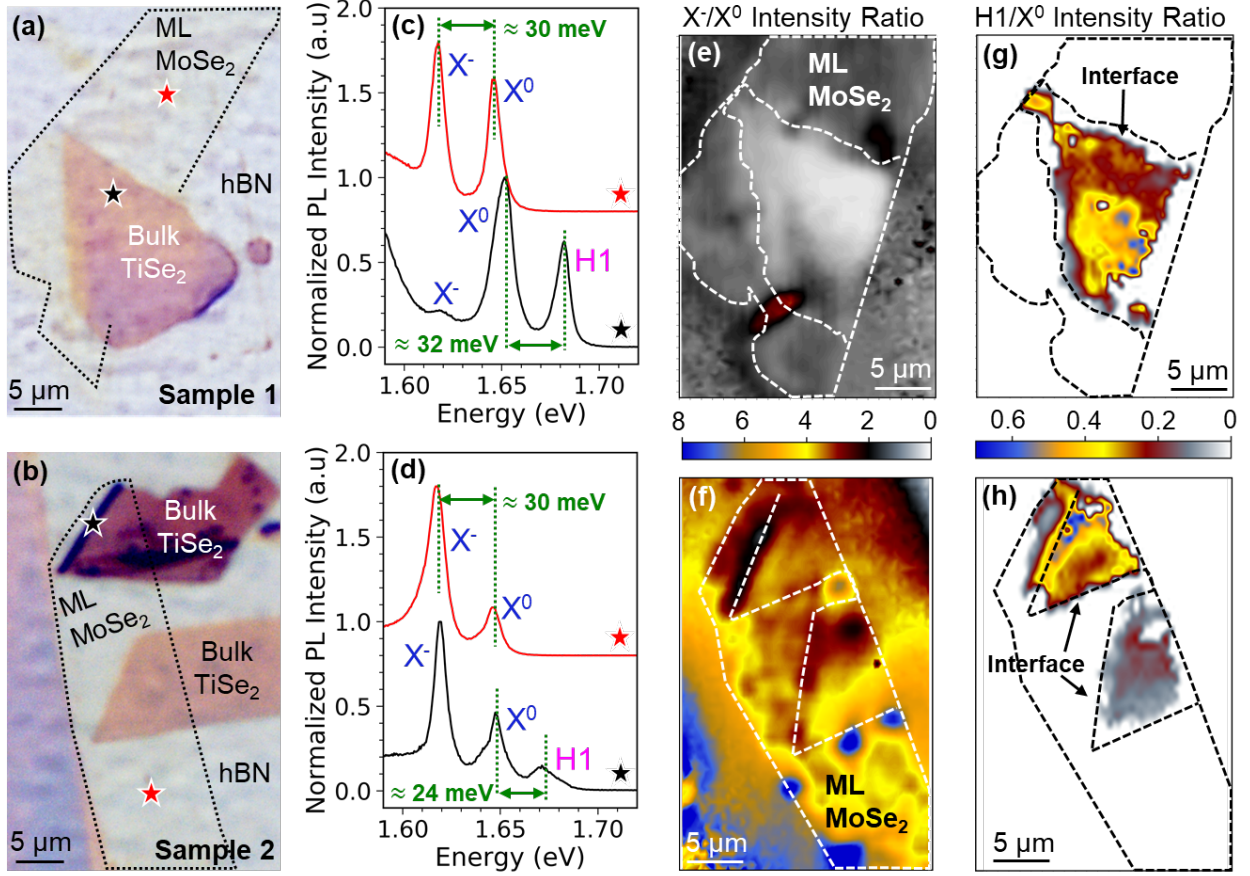


FIG. 1. Optical microscope images of TiSe_2 - MoSe_2 vdW heterostructures (a) Sample 1 and (b) Sample 2. The black dotted line outlines ML- MoSe_2 layer. Low-temperature (5 K) photoluminescence (PL) spectra taken on (black) and off (red) the interface for (c) Sample 1 and (d) Sample 2. These locations are denoted by red and black stars in panels (a) and (b), respectively. In addition to the X^0 and X^- emission observed in ML- MoSe_2 , the H1 PL peak appears at ≈ 1.68 eV on the interface. Spatially mapped X^-/X^0 integrated intensity ratio across the interface showing variations in the X^- intensity for (e) Sample 1 and (f) Sample 2. Spatially mapped H1/ X^0 integrated intensity ratio across the interface showing changes in H1 intensity in (g) Sample 1 and (h) Sample 2. The ratio X^-/X^0 correlates with changes in H1/ X^0 intensity at the junction.

be used as a proxy for interlayer spacing. MoSe_2 tends to be n -type as-exfoliated and TiSe_2 band alignment suggests it will act as an electron acceptor.⁵⁵ Therefore, the near absence of X^- emission on the Sample 1 overlap region suggests good coupling between the TiSe_2 - MoSe_2 flakes. For Sample 2 the X^-/X^0 ratio (Fig. 1(f)) is larger on the MoSe_2 flake, varying between 3-6, which may originate from unintentional doping during the heterostructure

fabrication process. On the TiSe₂ - MoSe₂ overlap we observe a reduction in X⁻ intensity co-localized with H1, but smaller than in Sample 1. From this we suggest that interlayer coupling is weaker in Sample 2 which could be due to contaminants or partial oxidation of the TiSe₂ flake. The remaining analyses will therefore focus on Sample 1, unless otherwise noted.

B. Temperature and power-dependence of H1

In this section we discuss temperature- and power-dependent PL measurements on and off the TiSe₂ - MoSe₂ interface. Figure 2(a) shows a temperature-dependent PL intensity map from 5 K- 265 K taken on the interface in Sample 1. A similar data set for Sample 2 is included in the Supplementary Information (Fig. S2). Here, the 5 K PL emission spectrum is the same as in Fig. 1(c) with prominent, sharp emission from X⁰ and H1, heavily reduced X⁻ emission and a broad feature originating from defects. With increasing temperature, PL from defect excitons and X⁻ decreases and becomes unobservable for $T > 70$ K in agreement with prior studies.⁵⁶⁻⁵⁹ Both X⁰ and H1 are visible at elevated temperatures, but are difficult to distinguish above ≈ 190 K. We obtain a better understanding through analysis of the PL lineshape for ML-MoSe₂ and TiSe₂ - MoSe₂. Figure 2(b) compares PL spectra at selected temperatures taken on (red curve) and off (black curve) the TiSe₂ - MoSe₂ interface. The presence of the TiSe₂ capping layer causes X⁰ to blueshift due to the different dielectric constant.^{25,26} To facilitate comparison, we eliminate this shift by adjusting the energy axis of the TiSe₂ - MoSe₂ spectrum so that the X⁰ PL peaks overlap. The energy shift amounts to ~ 1 -3 meV across the entire temperature range. H1 is visible as a weak shoulder of X⁰ between 190 K and 220 K. Above these temperatures, the PL lineshape on and off the interface is identical, indicating the driving mechanism behind H1 has dissipated. We also fit each PL spectrum to a sum of Lorentzian functions and extract the temperature-dependent peak parameters for H1, X⁰, and X⁻. The energy splitting, H1-X⁰, is shown in Fig. 2(c) over two cooling and warming runs that extend up to 200 K. In both cases the energy separation between H1 and X⁰ decreases with temperature until 200 K after which it is difficult to obtain a reliable fit.

The temperature window of 190 K – 220 K is apparently crucial to H1 and is known to be important for TiSe₂. Bulk 1T-TiSe₂ undergoes a $2 \times 2 \times 2$ commensurate-CDW

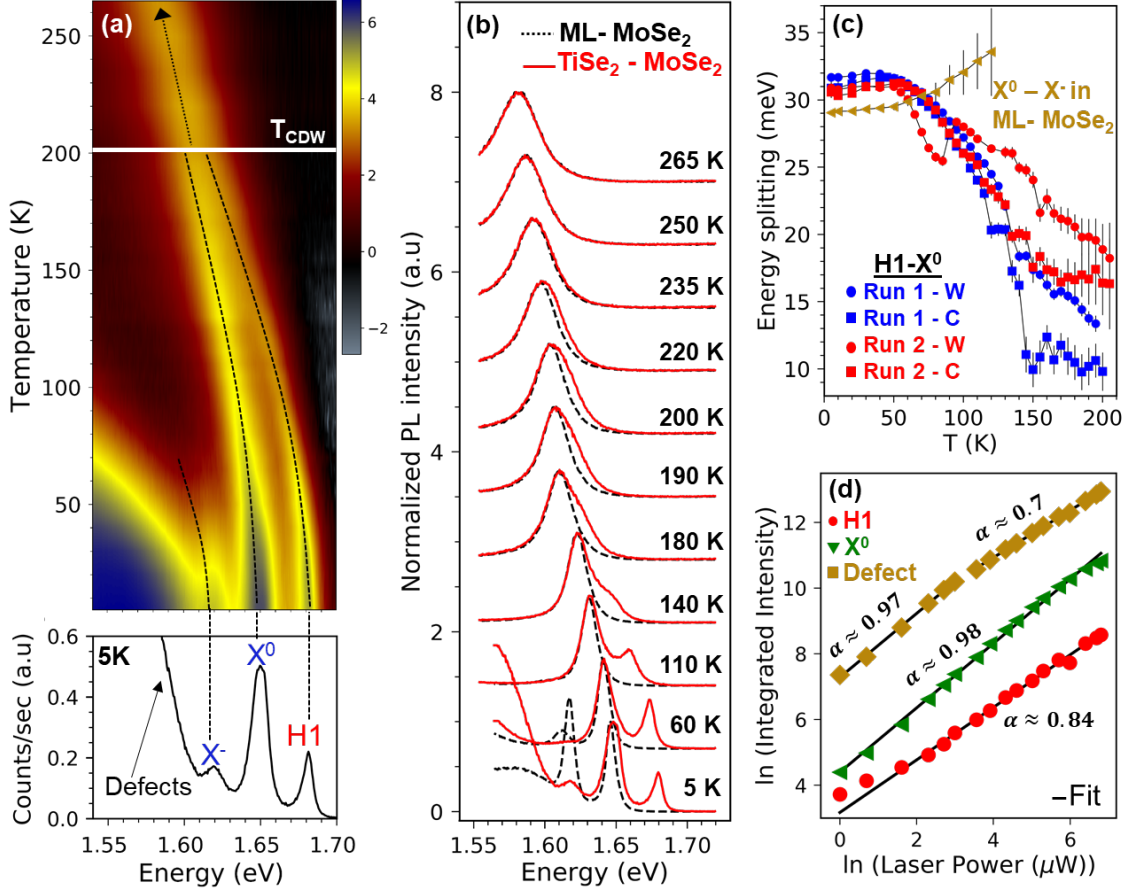


FIG. 2. (a) Temperature-dependent PL map on the TiSe_2 - MoSe_2 interface of Sample 1. The dashed lines are guides to the eye and the 5 K PL spectrum beneath the map labels the optical transitions. T_{CDW} for bulk TiSe_2 is indicated by the horizontal white line. (b) Lineshape analysis of PL spectra taken on (red) and off (black) the TiSe_2 - MoSe_2 interface. The interface spectra have been shifted to align the X^0 emission energies between the two curves. (c) Energy separation between H1 and X^0 versus temperature for two separate runs (red, blue), each consisting of a warming (W, circles) and cooling (C, squares) curve. $1-\sigma$ error bars from fits to the PL spectra are included. The X^0-X^- is included for ML- MoSe_2 to illustrate the difference from H1. (d) Log-log plot of the PL integrated intensity *versus* excitation laser power. The solid black lines are power-law fits to the data.

transition in the range of $T_{CDW} \approx 200$ K - 210 K, as observed in a variety of optical and electronic measurements.^{39,60-62} The CDW transition opens a band gap at the TiSe_2 M point in the Brillouin zone (BZ) with an associated order parameter well described by Bardeen-Cooper-Schrieffer (BCS) model.⁶² The observed correlation of H1 with T_{CDW} suggests a

close relationship between H1 in MoSe₂ and the CDW in TiSe₂.

Power-dependent PL measurements provide further insight into the nature of H1, as presented for Sample 1 in Fig. 2(d) and for Sample 2 in the Supporting Information (Fig. S2). PL intensity generally scales with power as $I_{PL} \propto P^\alpha$, where I_{PL} is the integrated PL intensity and P is the excitation power. The exponent $\alpha \approx 1$ for free excitons and > 1 for multiexcitons.¹⁶ Localized exciton states exhibit a more complicated behavior. At low powers $\alpha \sim 1$ but then becomes sublinear as the localized states are saturated.⁵⁹ These behaviors are observed in Fig. 2(d) where we plot the natural logarithms of I_{PL} and P . Linear fits to this data allow for the extraction of α . We find that both X⁰ and H1 have an $\alpha \approx 1$, with the value for H1 being somewhat lower, suggesting free exciton characteristics. As expected, the defect band first exhibits $\alpha \approx 1$ at low powers and then shows signs of saturation with $\alpha \approx 0.7$. While α for H1 is lower than would be expected for a free exciton, the absence of saturation is more consistent with this interpretation.

C. CDW phase at the TiSe₂ - MoSe₂ interface

Raman spectroscopy can probe the square of the CDW order parameter directly, since the intensity of the symmetry-forbidden modes appears in the second order of the ionic displacements of the high-symmetry positions. Raman measurements performed at the TiSe₂-MoSe₂ interface in the range of 5 - 265 K are shown in Fig. 3(a). The 5 K Raman spectra show the CDW modes at E_g^{CDW} (70 cm⁻¹) and A_g^{CDW} (108 cm⁻¹), as well as normal TiSe₂ lattice modes at 132 cm⁻¹ and 200 cm⁻¹ of E_g and A_{1g} symmetry, respectively.^{63,64} The MoSe₂ A_{1g} mode is also visible at 245 cm⁻¹ and is related to out-of-plane vibrations.⁶⁵ Figure 3(b) plots the temperature-dependent shifts of all TiSe₂ modes relative to their frequency at 5 K. The 135 cm⁻¹ mode is largely unaffected by temperature changes, blueshifting slightly as temperature is lowered and then stabilizing. The 200 cm⁻¹ mode is insensitive to the CDW transition and its anharmonicity can be understood by a combination of optical phonon decay and temperature-dependent changes in the lattice constants.⁶⁶ This is described by Eq. (1) (solid black line in Fig. 3(b)).

$$\Delta(\omega(0), T) = \omega_0 + A \left(1 + \frac{2}{e^x - 1} \right) \quad (1)$$

Here, $x = \hbar\omega_B/2k_B T$, ω_0 is the 0 K harmonic frequency and A represents the anharmonic contributions to the frequency of 200 cm⁻¹ optical mode as it decays into two acoustic

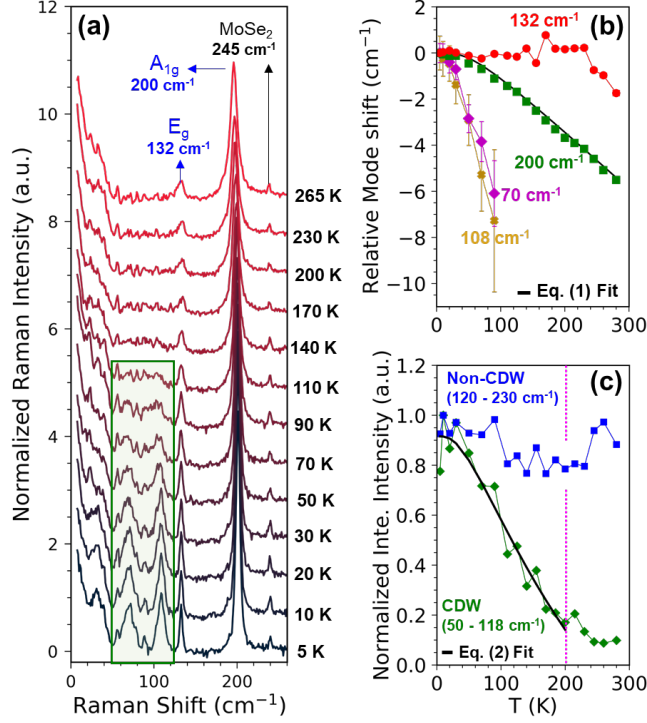


FIG. 3. (a) Temperature-dependent Raman spectra taken on the TiSe_2 - MoSe_2 interface in Sample 1. (b) Shift in the observed TiSe_2 Raman modes relative to the 5 K value. $1\text{-}\sigma$ error bars from spectral fitting included. The solid black line is fit to Eq. (1) that accounts for optical phonon decay processes (c) Normalized integrated Raman intensity of the CDW modes (green diamonds) and lattice modes (blue squares) versus temperature. The dotted magenta line indicates T_{CDW} . The solid black line is a fit to Eq. (2).

phonons. The obtained value for $A = -1.85 \text{ cm}^{-1}$ is within the ballpark of similar phonon anharmonicity studies done on TMDs.^{67,68}

The CDW modes at 70 cm^{-1} and 109 cm^{-1} redshift and broaden with increasing temperature. These modes are unresolved above $T = 100 \text{ K}$, which is well below T_{CDW} . This behavior is commonly attributed to quantum fluctuations of the density wave.⁶⁹ Integrating the Raman intensity over the spectral range encompassing the CDW modes allows us to monitor the CDW up to the transition temperature (Fig. 3(c)). Thermal melting of the CDW is expected to follow a temperature dependence consistent with the BCS treatment where the order parameter $\Delta(T)$ can be given as⁷⁰

$$\frac{\Delta^2(T)}{\Delta^2(0)} \propto \tanh^2 \left(\alpha_{BCS} \sqrt{1 - \frac{T}{T_{CDW}}} \right), \quad (2)$$

This model fits the integrated intensity data well up to T_{CDW} as shown in Fig. 3(c).

III. DISCUSSION

Investigations into the properties of 2D excitons in TMDs have covered remarkable ground over the past decade.^{9,71–73} Despite these remarkably comprehensive studies, no observations of vdW heterostructures have shown PL satellites above X^0 . Therefore, we explore here three possible mechanisms that could be responsible for H1.

Before proceeding with the analysis of potential microscopic interpretations of the new peak, we summarize key experimental observations. First, H1 lies 25–32 meV above X^0 with an intensity that differs between samples (Fig. 1). Second, within a single sample the relative intensity of H1 to X^0 is temperature independent (Fig. 4(a)). Third, the energy difference between H1 and X^0 follows the CDW order parameter Δ^2 . We illustrate this in Fig. 4(c) by overlaying neutron scattering data from Ref.61, the energy separation H1– X^0 , and the integrated intensity of the TiSe₂-CDW Raman features. Fourth, the intensity ratio H1/ X^0 decreases with increasing laser power (Fig. 4(b)). And lastly, H1 and X^- are spatially anti-correlated (Fig. 1).

A. Mechanism I: Activation of Forbidden/Dark Excitons

Semiconducting TMDs host numerous dark exciton states where optical recombination is forbidden by momentum conservation or symmetry. Density functional theory (DFT) calculations of MoSe₂ suggest a finite-momentum dark exciton lies 30 meV above X^0 .⁷⁴ This indirect exciton is formed from an electron residing at the $Q(Q')$ valley and a hole at the $K(K')$ valley (Fig. 4(e)). The indirect exciton has not been observed experimentally in PL, but resonant Raman measurements offers some evidence for dark excitons above X^0 .⁷⁵ While the energy of this exciton matches the energy of H1, a viable mechanism is required to provide the missing momentum needed for optical recombination of this dark state. Mechanism I explores how the interface between TiSe₂ and MoSe₂ could potentially activate such dark states by introducing a new spatial periodicity that violates quasimomentum conservation.

MoSe₂ and TiSe₂ form an incommensurate superstructure for most stacking configurations, which, formally, implies a full relaxation of quasimomentum conservation. In order to

illustrate this, consider the MoSe₂ Bloch wave functions at the TiSe₂ - MoSe₂ overlap. We assume there is no hybridization between MoSe₂ and TiSe₂ wave functions, which is reasonable due to their large spatial separation. The quasimomentum can then be defined by the MoSe₂ lattice alone and the Bloch functions are $\psi_{\mathbf{k}}(\mathbf{r}) = \sum_{\mathbf{g}} a_{\mathbf{k}+\mathbf{g}} \exp[i(\mathbf{k} + \mathbf{g}) \cdot \mathbf{r}]$, where \mathbf{g} is a MoSe₂ reciprocal lattice (r.l.) vector and $a_{\mathbf{k}+\mathbf{g}}$ are the Bloch coefficients. The presence of the TiSe₂ lattice and CDW can be thought of as a periodic “defect” for MoSe₂ that enables scattering between the K and Q points. The matrix element of the associated potential for Bloch states is $\langle \psi_{\mathbf{Q}} | V(\mathbf{r}) | \psi_{\mathbf{K}} \rangle$, where \mathbf{K} is a wavevector for any of the K -equivalent points and \mathbf{Q} is a wavevector for any of the Q -equivalent ones (Fig. 4(e)). $V(\mathbf{r})$ is the effective TiSe₂ defect potential, which can be expanded in the TiSe₂ r.l. vectors \mathbf{t} . Note that the lattice parameter for TiSe₂ is 7.8% larger than MoSe₂, so that if we measure the reciprocal space in units of $2\pi/a_{\text{MoSe}_2}$, then for Mo the first r.l. vectors will be $\mathbf{g}_{1,2} = \{\sqrt{3}/2, \pm 1/2\}$; $\mathbf{g}_3 = \mathbf{g}_1 + \mathbf{g}_2$. For TiSe₂, the equivalent r.l. vectors $\mathbf{t}_{1,2,3}$ will be shorter by 7.8%.

Using the expansion of $V(\mathbf{r})$ we obtain,

$$\begin{aligned}
\langle \psi_{\mathbf{Q}} | V(\mathbf{r}) | \psi_{\mathbf{K}} \rangle &= \sum_{\mathbf{t}} \langle \psi_{\mathbf{Q}} | v_{\mathbf{t}} e^{i\mathbf{t} \cdot \mathbf{r}} | \psi_{\mathbf{K}} \rangle \\
&= \sum_{\mathbf{t}, \mathbf{g}, \mathbf{g}'} \left\langle a_{\mathbf{K}+\mathbf{g}} e^{i(\mathbf{K}+\mathbf{g}) \cdot \mathbf{r}} v_{\mathbf{t}} e^{i\mathbf{t} \cdot \mathbf{r}} a_{\mathbf{Q}+\mathbf{g}'}^* e^{-i(\mathbf{Q}+\mathbf{g}') \cdot \mathbf{r}} \right\rangle \\
&= \sum_{\mathbf{t}, \mathbf{K}, \mathbf{Q}} a_{\mathbf{K}} a_{\mathbf{Q}}^* v_{\mathbf{t}} \langle e^{i(\mathbf{K}-\mathbf{Q}+\mathbf{t}) \cdot \mathbf{r}} \rangle \\
&= \sum_{\mathbf{t}, \mathbf{K}, \mathbf{Q}} a_{\mathbf{K}} a_{\mathbf{Q}}^* v_{\mathbf{t}} \delta(\mathbf{K} - \mathbf{Q} + \mathbf{t}).
\end{aligned}$$

In the last line the summation goes over all equivalent K and Q points. While, in principle, in an infinite lattice one can always find a triad $\mathbf{K}, \mathbf{Q}, \mathbf{t}$ wavevectors that closely satisfies the condition $|\mathbf{K} - \mathbf{Q} + \mathbf{t}| = \mathbf{0}$, the coefficients $v_{\mathbf{t}}$, and, to lesser extent, $a_{\mathbf{g}}$, rapidly decay (the form factor effect), and so this scattering process can only be efficient if t is small.

Determining if the TiSe₂ ”defect“ potential can enable $K \rightarrow Q$ scattering requires matching $|\mathbf{t}|$ and $|\mathbf{K} - \mathbf{Q}|$. We have carried out DFT calculations of the TiSe₂ - MoSe₂ heterostructure to determine how this position is altered by interlayer coupling. The location of the Q valley is $\kappa = |\mathbf{Q} - \mathbf{\Gamma}|/|\mathbf{K} - \mathbf{\Gamma}|$, which are clustered around 0.55 ± 0.05 for multiple DFT runs. The magnitude of the smallest scattering vectors $\mathbf{K} - \mathbf{Q}$ are: $(1 - \kappa)/\sqrt{3}$, $(1 + \kappa)/\sqrt{3}$, $(\sqrt{1 - \kappa + \kappa^2})/\sqrt{3}$, $(\sqrt{1 + \kappa + \kappa^2})/\sqrt{3}$, $(2 - \kappa)/\sqrt{3}$ and $(\sqrt{4 - 2\kappa + \kappa^2})/\sqrt{3}$, where the first two values correspond to scattering from Q to K or K' , while the next two to scat-

tering from Q' to K or K' , and the last two to scattering into the next BZ. For $\kappa = 0.55$, in units of $2\pi/a_{\text{MoSe}_2}$, these are 0.260, 0.895, 0.501, 0.785, 0.832, and 1.033, respectively. At the same time, the smallest vector of the r.l. of TiSe_2 without the CDW is $t_1 = 0.928(2\pi/a_{\text{Mo}})$.

In Fig. 4(e) we present the magnitude of the scattering wavevector $|\mathbf{K} - \mathbf{Q}|$ between different K and Q points versus κ in MoSe_2 . These are compared to the r.l. vectors of TiSe_2 in the normal (blue dots) and CDW (red dot) phases. The smallest TiSe_2 r.l. vector can only match one of the $|\mathbf{K} - \mathbf{Q}|$ values if κ is 0.607, which is far outside our DFT predictions. In the $2 \times 2 \times 2$ CDW phase of TiSe_2 , the magnitude of the r.l. vectors (τ_i) are shortened to : $\tau_1 = t_1/2$; $\tau_2 = t_1\sqrt{3}/2$; $\tau_3 = t_1$; $\tau_4 = \sqrt{7}/2t_1$. We find that particularly $\tau_2 = 0.804$ is close to the magnitude of one of the $\mathbf{K} - \mathbf{Q}$ vectors. This is shown by the red dot in Fig. 4(e). The mismatch is less than $0.019(2\pi/a_{\text{Mo}})$ and is reduced to zero for $\kappa = 0.59$, a value within the range of the DFT calculations.

Therefore we conclude that the CDW potential opens a new $K \rightarrow Q$ scattering channel. This would enable optical recombination of an indirect, finite momentum exciton resulting in the appearance of a new PL line at the same energy as H1.⁷⁴ Future calculations taking into account the effect of the CDW-exciton coupling may be able to assess this scenario quantitatively, but such calculations are outside our current capabilities. This result explains the emission energy of H1, its disappearance at T_{CDW} , and its anticorrelation with X^- . However, this mechanism would also imply that H1- X^0 (barring unrelated phenomena) to be T -independent and the H1/ X^0 intensity ratio to follow Δ^2 . Our observations indicate just the opposite (Fig. 4(a) and 4(c)). Furthermore, this mechanism cannot explain the decrease in the H1/ X^0 intensity ratio with excitation power in Fig. 4(b).

B. Mechanism II: Interlayer 2D TiSe_2 - MoSe_2 Exciton

Another intriguing possibility is the formation of an interlayer exciton by an electron in MoSe_2 and a hole in TiSe_2 layer as shown in Fig. 4(d). This is only possible due to the opening of the CDW band-gap in the low-temperature regime, but is inconceivable in the normal metallic phase. The intensity of such an exciton will be defined by (T -independent) interlayer tunneling, and the position will be, roughly, given by $E_c(\text{MoSe}_2) - E_F(\text{TiSe}_2) - E_{CDW}(\text{TiSe}_2)/2$. The energy gap, E_{CDW} , is proportional to the order parameter Δ^2 , and its value is unclear: experiments cite different numbers, most ARPES studies find the top

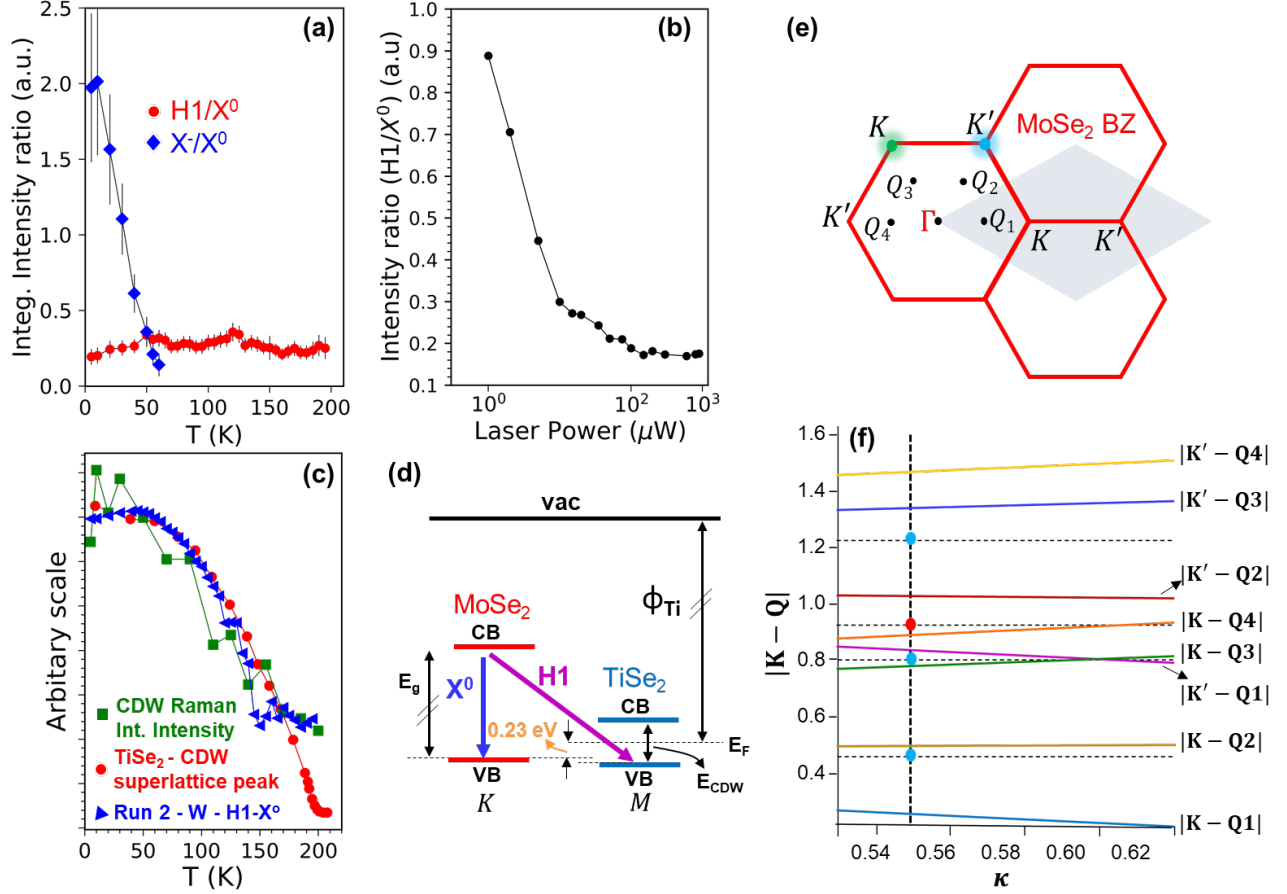


FIG. 4. (a) PL integrated intensity ratios $H1/X^0$ (red circles) and X^-/X^0 (blue diamonds) versus temperature. (b) $H1/X^0$ integrated intensity ratio versus the laser power (lin-log scale). (c) Overlay of the energy separation between $H1$ and X^0 for Sample 1, the integrated Raman intensity of the CDW modes and the $TiSe_2$ -CDW superlattice peak extracted from neutron scattering data in Ref. 61, all as a function of temperature. (d) A schematic of a type-II band alignment at the $TiSe_2$ - $MoSe_2$ interface leading to an interlayer exciton. (e) Brillouin zones for the $MoSe_2$ lattice and the corresponding r.l. unit cell (gray). (f) Lengths of the scattering vectors $|\mathbf{K} - \mathbf{Q}|$ in units of the $MoSe_2$ reciprocal lattice (r.l.) vectors (colored solid lines) compared to the length of the reciprocal lattice vectors of the undistorted (red dot) and CDW (blue dots) $TiSe_2$. The horizontal dashed lines are guides to the eye. The vertical dashed line is drawn to pass through $\kappa = 0.55$, to facilitate the comparison with the magnitude of the $MoSe_2$ wavevectors $|\mathbf{K} - \mathbf{Q}|$ and the smallest r.l. vector (dots) in $TiSe_2$.

of the valence band to be separated from the Fermi level (*i.e.*, half the band gap) by 50–75

meV,^{62,76} qualitatively consistent with the H1–X⁰ separation, and roughly following Δ^2 .

For this scenario to be realized the top of the Mo valence band at K should fall inside the CDW gap in TiSe₂ (or, equivalently, within a few tens of meV from the TiSe₂ Fermi energy, E_F , in the metallic phase). Our standard DFT calculations using a supercell with 2×2 periodicity in TiSe₂ and $\sqrt{7} \times \sqrt{39}$ in MoSe₂ (Ti₁₆Mo₁₉) show that E_F is about 230 meV above the MoSe₂ valence band. This is illustrated in Fig. 4(d) and detailed in Supporting Information Section S4. So, while this naturally explains all five experimental observation, it also requires an assumption that the DFT calculations of the band alignment are off by 100–150 meV, which may be reasonable once the electronic correlations that drive CDW formation and the details of the vdW interface are properly included.

C. Mechanism III: Exciton-Phonon and Exciton-Plasmon Interaction

Exciton formation and recombination can in principle be assisted through coupling to a variety of bosonic excitations. Again focusing on the activation of a dark finite-momentum exciton, the lowest energy phonon with the appropriate momentum has an energy of ~ 10 meV,⁷⁷ so that the corresponding PL energy should be shifted down (phonon-assisted emission) from the momentum-dark exciton energy. This would suggest that H1 is a phonon replica of a higher energy exciton, either symmetry forbidden or momentum-indirect. However, this mechanism is unlikely considering that it is intrinsic to MoSe₂ and cannot explain the role of the TiSe₂ CDW. In principle, interlayer coupling could allow TiSe₂ phonons to create exciton-phonon replicas in MoSe₂. H1 should in this case emerge at higher temperature if TiSe₂ phonons are involved and the replica would show additional temperature dependence compared to X⁰, in contradiction with our observation.^{78–80} An additional possibility regarding the activation of a finite-momentum exciton by coupling to TiSe₂ is the presence of a distinct low-energy plasmon. A curious aspect of the TiSe₂-CDW transition is the presence of a low-energy plasmon, which has been claimed as evidence of the excitonic insulator mechanism,⁸¹ although this claim was later disputed.⁸² This plasmon was measured to have an energy of $\hbar\omega_{pl}(q) \approx 50$ meV at $T = 17$ K with $q = 0$. This excitation was found to soften with temperature, reaching $\hbar\omega_{pl} \approx 35$ meV at $T = 185$ K. The plasmon is only present in the CDW phase, so it is tempting to associate it with the H1 PL line.

Signatures of exciton-plasmon interaction in PL have attracted considerable attention

recently.⁸³⁻⁸⁶ While these papers consider excitons and plasmons spatially coexisting in the same material, the theory is equally applicable to spatially separated MoSe₂ excitons and TiSe₂ plasmons, as long as they are coupled by Coulomb interaction. In principle, two mechanisms are possible (see Supporting Information - Section S3 for a detailed discussion): the exciton Green function can be renormalized by a virtual process of emission and absorption of a plasmon or a process with either emission or absorption of a real plasmon. The former process shifts the exciton line E_X up by a fixed amount, which in the first approximation can be expressed as $E_X^2 - E_{X0}^2 \approx 4|\mathcal{M}|^2 E_{X0} \hbar\omega_{pl} / (E_{X0}^2 - (\hbar\omega_{pl})^2) \approx 4|\mathcal{M}|^2 \hbar\omega_{pl} / E_{X0}$, where E_{X0} is the position of X^0 in the absence of exciton-plasmon coupling and \mathcal{M} is the exciton-plasmon coupling constant. However, one would expect the coupling constant to vary spatially, so instead of two lines one would observe a broad manifold starting at E_{X0} and ending at around $E_{X0} + 2|\mathcal{M}|^2 \hbar\omega_{pl} / E_{X0}$, in contradiction with the experiment. The other mechanism preserves the main line and adds two satellites, shifted down and up by around ω_{pl} . The intensity of the upper peak is roughly temperature independent, and the intensity of the lower peak is proportional to the population of thermally or extrinsically excited plasmons. We do not observe the lower satellite at all, and the upper satellite, H1, only loses its intensity with temperature (Fig. 2(b)) and with the laser power (Fig. 4(b)), in obvious contradiction with the assumed physics.

IV. CONCLUSION

We have discovered the presence of a new exciton-like peak in TiSe₂ - MoSe₂ heterostructures using temperature-dependent PL spectroscopy. The H1 emission feature is localized to the heterostructure interface and correlated with T_{CDW} in TiSe₂. We have presented multiple scenarios that could explain the origin of this feature. The most plausible explanations of H1 are, presently, 1) an interlayer TiSe₂ - MoSe₂ exciton and 2) the brightening of momentum dark excitons by the CDW potential. These results are the first demonstration of exciton engineering via proximitized CDWs and provide the 2D theoretical community with a fresh challenge to understand the microscopic mechanisms underlying CDW-exciton interactions.

V. GROWTH OF TMD MATERIALS

MoSe₂ crystals were grown by the chemical vapor transport (CVT) method using polycrystalline MoSe₂ powder (≈ 1 g) and SeBr₄ transport agent (≈ 0.1 g). The source and growth zones in a vacuum-sealed 20 cm long quartz ampoule were kept at 980 °C and 890 °C, respectively, for 7 days. The procedure for CVT-grown TiSe₂ crystals is outlined in Ref. 39.

VI. SAMPLE PREPARATION, ASSEMBLY AND AFM ‘NANO-SQUEEGEE’

Bulk-hBN flakes were mechanically exfoliated and transferred on O₂ plasma cleaned Si/SiO₂ substrates. MLs of 2H-MoSe₂ obtained through mechanical exfoliation were subsequently transferred on an identified hBN flake. For both materials, the transfer process was done using the PDMS-based dry viscoelastic stamping method.⁴⁹ This method has been known to leave polymer residue between the interface of two TMDs deposited during the transfer process, but has proven to be optimal for fabricating heterostructures.⁷ To create clean interfaces, an AFM-based ‘nano-squeegee’ procedure was employed.⁵⁰ This involves the use of a standard AFM tip to push out polymer residue deposited between the two TMDs in a vertical heterostructure. We were able to use the same method to also remove surface residue present on the ML-MoSe₂ flake, using a 7 N/m spring constant tip and a contact force of 140 nN. Bulk TiSe₂ is then brought into contact with the sample using the same dry-transfer technique as done for ML-MoSe₂. The sample was additionally vacuum annealed at 200 °C for 5 hours to improve coupling.

VII. EXPERIMENTAL SETUP

Low-temperature PL and Raman measurements were carried out on a home-built confocal microscope setup with 532 nm laser excitation focused through a 0.42 NA, 50x long working-distance objective to achieve a spot diameter of 2.4 μ m. The light is collected in a back-scattering geometry, with the collection fiber-coupled to a 500 mm focal length single spectrometer integrated with a liquid-N₂ cooled CCD detector. The samples were placed under vacuum and cooled in a closed cycle He-cooled cryostat (Montana Instruments Cor-

poration) with a variable temperature range from 4 K - 300 K. Raman measurements on the TiSe_2 - MoSe_2 interface were carried out using the same collection scheme, however, the excitation path included a collection of Bragg grating notch filters to get us within 15 cm^{-1} of the laser line. The excitation wavelength used for Raman measurements was 532 nm and the laser power was kept at $300 \mu\text{W}$ pre-objective. Spatially-resolved and temperature-dependent PL measurements were done using the same laser wavelength while the power was kept within $150 \mu\text{W}$ pre-objective.

VIII. ACKNOWLEDGEMENT

P.M.V. and J.J. acknowledge support from the National Science Foundation (NSF) under Grant No. DMR-1748650 and DMR-1847782, and the George Mason University Quantum Science and Engineering Center. This work is partly supported through the Material Genome Initiative funding allocated to NIST. I.Ž. was supported by the U.S. DOE, Office of Science BES, Award No. DE-SC0004890. We acknowledge valuable discussions with Madeleine Phillips and Steven Hellberg. Materials synthesis at the University of Maryland Quantum Materials Center was supported by the Gordon and Betty Moore Foundation's EPiQS Initiative through Grant No. GBMF9071.

IX. DISCLAIMER

Certain commercial equipment, instruments, or materials are identified in this paper in order to specify the experimental procedure adequately. Such identification is not intended to imply recommendation or endorsement by the National Institute of Standards and Technology, nor is it intended to imply that the materials or equipment identified are necessarily the best available for the purpose.

X. DATA AVAILABILITY STATEMENT

The data that support the findings of this study are available from the corresponding author upon reasonable request.

REFERENCES

- ¹I. Žutić, A. Matos-Abiague, B. Scharf, H. Dery, and K. Belashchenko, “Proximitized materials,” *Mater. Today* **22**, 85–107 (2019).
- ²A. K. Geim and I. V. Grigorieva, “Van der Waals heterostructures,” *Nature* **499**, 419–425 (2013).
- ³R. Bistritzer and A. H. MacDonald, “Moiré bands in twisted double-layer graphene,” *Proc. Natl. Acad. Sci. U. S. A.* **108**, 12233–12237 (2011).
- ⁴Y. Cao, V. Fatemi, S. Fang, K. Watanabe, T. Taniguchi, E. Kaxiras, and P. Jarillo-Herrero, “Unconventional superconductivity in magic-angle graphene superlattices,” *Nature* **556**, 43–50 (2018).
- ⁵K. Tran, G. Moody, F. Wu, X. Lu, J. Choi, K. Kim, A. Rai, D. A. Sanchez, J. Quan, A. Singh, J. Embley, A. Zepeda, M. Campbell, T. Autry, T. Taniguchi, K. Watanabe, N. Lu, S. K. Banerjee, K. L. Silverman, S. Kim, E. Tutuc, L. Yang, A. H. MacDonald, and X. Li, “Evidence for moiré excitons in van der Waals heterostructures,” *Nature* **567**, 71–75 (2019).
- ⁶H. Yu, G.-B. Liu, J. Tang, X. Xu, and W. Yao, “Moiré excitons: From Programmable Quantum Emitter Arrays to Spin-Orbit-Coupled Artificial Lattices,” *Sci. Adv.* **3**, e1701696 (2017).
- ⁷R. Frisenda, E. Navarro-Moratalla, P. Gant, D. Pérez De Lara, P. Jarillo-Herrero, R. V. Gorbachev, and A. Castellanos-Gomez, “Recent Progress in the Assembly of Nanodevices and van der Waals Heterostructures by Deterministic Placement of 2D Materials,” *Chem. Soc. Rev.* **47**, 53–68 (2018).
- ⁸M. Onodera, S. Masubuchi, R. Moriya, and T. Machida, “Assembly of van der Waals heterostructures: exfoliation, searching, and stacking of 2D materials,” *Jpn. J. Appl. Phys.* **59**, 010101 (2020).
- ⁹G. Wang, A. Chernikov, M. M. Glazov, T. F. Heinz, X. Marie, T. Amand, and B. Urbaszek, “Colloquium : Excitons in atomically thin transition metal dichalcogenides,” *Rev. Mod. Phys.* **90**, 021001 (2018).
- ¹⁰T. Mueller and E. Malic, “Exciton physics and device application of two-dimensional transition metal dichalcogenide semiconductors,” *npj 2D Mater. Appl.* **2**, 29 (2018).

- ¹¹J. S. Ross, S. Wu, H. Yu, N. J. Ghimire, A. M. Jones, G. Aivazian, J. Yan, D. G. Mandrus, D. Xiao, W. Yao, and X. Xu, “Electrical control of neutral and charged excitons in a monolayer semiconductor,” *Nat. Commun.* **4**, 1474 (2013).
- ¹²Z. Li, T. Wang, S. Miao, Z. Lian, and S.-F. Shi, “Fine structures of valley-polarized excitonic states in monolayer transitional metal dichalcogenides,” *Nanophotonics* **9**, 1811–1829 (2020).
- ¹³Z. Li, T. Wang, Z. Lu, C. Jin, Y. Chen, Y. Meng, Z. Lian, T. Taniguchi, K. Watanabe, S. Zhang, D. Smirnov, and S.-F. Shi, “Revealing the biexciton and trion-exciton complexes in BN encapsulated WSe₂,” *Nat. Commun.* **9**, 3719 (2018).
- ¹⁴Z. Ye, L. Waldecker, E. Y. Ma, D. Rhodes, A. Antony, B. Kim, X.-X. Zhang, M. Deng, Y. Jiang, Z. Lu, D. Smirnov, K. Watanabe, T. Taniguchi, J. Hone, and T. F. Heinz, “Efficient generation of neutral and charged biexcitons in encapsulated WSe₂ monolayers,” *Nat. Commun.* **9**, 3718 (2018).
- ¹⁵S.-Y. Chen, T. Goldstein, T. Taniguchi, K. Watanabe, and J. Yan, “Coulomb-Bound Four- and Five-Particle Intervalley States in an Atomically-Thin Semiconductor,” *Nat. Commun.* **9**, 3717 (2018).
- ¹⁶M. Barbone, A. R.-P. Montblanch, D. M. Kara, C. Palacios-Berraquero, A. R. Cadore, D. De Fazio, B. Pingault, E. Mostaani, H. Li, B. Chen, K. Watanabe, T. Taniguchi, S. Tongay, G. Wang, A. C. Ferrari, and M. Atatüre, “Charge-Tuneable Biexciton Complexes in Monolayer WSe₂,” *Nat. Commun.* **9**, 3721 (2018).
- ¹⁷C. Robert, B. Han, P. Kapuscinski, A. Delhomme, C. Faugeras, T. Amand, M. R. Molas, M. Bartos, K. Watanabe, T. Taniguchi, B. Urbaszek, M. Potemski, and X. Marie, “Measurement of the spin-forbidden dark excitons in MoS₂ and MoSe₂ monolayers,” *Nat. Commun.* **11**, 4037 (2020).
- ¹⁸Z. Lu, D. Rhodes, Z. Li, D. V. Tuan, Y. Jiang, J. Ludwig, Z. Jiang, Z. Lian, S.-F. Shi, J. Hone, H. Dery, and D. Smirnov, “Magnetic Field Mixing and Splitting of Bright and Dark Excitons in Monolayer MoSe₂,” *2D Mater.* **7**, 15017 (2019).
- ¹⁹E. Malic, M. Selig, M. Feierabend, S. Brem, D. Christiansen, F. Wendler, A. Knorr, and G. Berghäuser, “Dark excitons in transition metal dichalcogenides,” *Phys. Rev. Mater.* **2**, 014002 (2018).
- ²⁰X. X. Zhang, T. Cao, Z. Lu, Y. C. Lin, F. Zhang, Y. Wang, Z. Li, J. C. Hone, J. A. Robinson, D. Smirnov, S. G. Louie, and T. F. Heinz, “Magnetic brightening and control

- of dark excitons in monolayer WSe₂,” *Nat. Nanotechnol.* **12**, 883–888 (2017).
- ²¹W.-t. Hsu, J. Quan, C.-y. Wang, L.-s. Lu, M. Campbell, W.-h. Chang, L.-J. Li, X. Li, and C.-K. Shih, “Dielectric Impact on Exciton Binding Energy and Quasiparticle Bandgap in Monolayer WS₂ and WSe₂,” *2D Mater.* **6**, 025028 (2019).
- ²²M. Florian, M. Hartmann, A. Steinhoff, J. Klein, A. W. Holleitner, J. J. Finley, T. O. Wehling, M. Kaniber, and C. Gies, “The Dielectric Impact of Layer Distances on Exciton and Trion Binding Energies in van der Waals Heterostructures,” *Nano Lett.* **18**, 2725–2732 (2018).
- ²³S. Borghardt, J.-S. Tu, F. Winkler, J. Schubert, W. Zander, K. Leosson, and B. E. Kardynal, “Engineering of Optical and Electronic Bandgaps in Transition Metal Dichalcogenide Monolayers through External Dielectric Screening,” *Phys. Rev. Mater.* **1**, 054001 (2017).
- ²⁴A. V. Stier, N. P. Wilson, G. Clark, X. Xu, and S. A. Crooker, “Probing the Influence of Dielectric Environment on Excitons in Monolayer WSe₂: Insight from High Magnetic Fields,” *Nano Lett.* **16**, 7054–7060 (2016).
- ²⁵A. Raja, A. Chaves, J. Yu, G. Arefe, H. M. Hill, A. F. Rigosi, T. C. Berkelbach, P. Nagler, C. Schüller, T. Korn, C. Nuckolls, J. Hone, L. E. Brus, T. F. Heinz, D. R. Reichman, and A. Chernikov, “Coulomb engineering of the bandgap and excitons in two-dimensional materials,” *Nat. Commun.* **8**, 15251 (2017).
- ²⁶A. Raja, L. Waldecker, J. Zipfel, Y. Cho, S. Brem, J. D. Ziegler, M. Kulig, T. Taniguchi, K. Watanabe, E. Malic, T. F. Heinz, T. C. Berkelbach, and A. Chernikov, “Dielectric disorder in two-dimensional materials,” *Nat. Nanotechnol.* **14**, 832–837 (2019).
- ²⁷Y. Jiang, S. Chen, W. Zheng, B. Zheng, and A. Pan, “Interlayer exciton formation, relaxation, and transport in TMD van der Waals heterostructures,” *Light Sci. Appl.* **10**, 72 (2021).
- ²⁸A. T. Hanbicki, H.-J. Chuang, M. R. Rosenberger, C. S. Hellberg, S. V. Sivaram, K. M. McCreary, I. I. Mazin, and B. T. Jonker, “Double Indirect Interlayer Exciton in a MoSe₂/WSe₂ van der Waals Heterostructure,” *ACS Nano* **12**, 4719–4726 (2018).
- ²⁹B. Miller, A. Steinhoff, B. Pano, J. Klein, F. Jahnke, A. Holleitner, and U. Wurstbauer, “Long-Lived Direct and Indirect Interlayer Excitons in van der Waals Heterostructures,” *Nano Lett.* **17**, 5229–5237 (2017).

- ³⁰N. Zhang, A. Surrente, M. Baranowski, D. K. Maude, P. Gant, A. Castellanos-Gomez, and P. Plochocka, “Moiré Intralayer Excitons in a MoSe₂/MoS₂ Heterostructure,” *Nano Lett.* **18**, 7651–7657 (2018).
- ³¹T. Norden, C. Zhao, P. Zhang, R. Sabirianov, A. Petrou, and H. Zeng, “Giant valley splitting in monolayer WS₂ by magnetic proximity effect,” *Nat. Commun.* **10**, 4163 (2019).
- ³²L. Ciorciaro, M. Kroner, K. Watanabe, T. Taniguchi, and A. Imamoglu, “Observation of Magnetic Proximity Effect Using Resonant Optical Spectroscopy of an Electrically Tunable MoSe₂/CrBr₃ Heterostructure,” *Phys. Rev. Lett.* **124**, 197401 (2020).
- ³³B. Scharf, G. Xu, A. Matos-Abiague, and I. Žutić, “Magnetic Proximity Effects in Transition-Metal Dichalcogenides: Converting Excitons,” *Phys. Rev. Lett.* **119**, 127403 (2017).
- ³⁴D. Zhong, K. L. Seyler, X. Linpeng, R. Cheng, N. Sivadas, B. Huang, E. Schmidgall, T. Taniguchi, K. Watanabe, M. A. McGuire, W. Yao, D. Xiao, K.-M. C. Fu, and X. Xu, “Van der Waals engineering of ferromagnetic semiconductor heterostructures for spin and valleytronics,” *Sci. Adv.* **3**, e1603113 (2017).
- ³⁵G. Xu, T. Zhou, B. Scharf, and I. Žutić, “Optically Probing Tunable Band Topology in Atomic Monolayers,” *Phys. Rev. Lett.* **125**, 157402 (2020).
- ³⁶Y. Zhou, J. Sung, E. Brutschea, I. Esterlis, Y. Wang, G. Scuri, R. J. Gelly, H. Heo, T. Taniguchi, K. Watanabe, G. Zaránd, M. D. Lukin, P. Kim, E. Demler, and H. Park, “Bilayer Wigner crystals in a transition metal dichalcogenide heterostructure,” *Nature* **595**, 48–52 (2021).
- ³⁷E. Liu, T. Taniguchi, K. Watanabe, N. M. Gabor, Y.-T. Cui, and C. H. Lui, “Excitonic and valleytronic signatures of correlated states at fractional fillings of a moiré superlattice,” *Phys. Rev. Lett.* **127**, 037402 (2020).
- ³⁸S. Miao, T. Wang, X. Huang, D. Chen, Z. Lian, C. Wang, M. Blei, T. Taniguchi, K. Watanabe, S. Tongay, Z. Wang, D. Xiao, Y.-T. Cui, and S.-F. Shi, “Strong interaction between interlayer excitons and correlated electrons in WSe₂/WS₂ moiré superlattice,” *Nature Communications* **12**, 3608 (2021).
- ³⁹D. J. Campbell, C. Eckberg, P. Y. Zavalij, H.-H. Kung, E. Razzoli, M. Michiardi, C. Jozwiak, A. Bostwick, E. Rotenberg, A. Damascelli, and J. Paglione, “Intrinsic insulating ground state in transition metal dichalcogenide TiSe₂,” *Phys. Rev. Mater.* **3**, 053402 (2019).

- ⁴⁰K. Rossnagel, L. Kipp, and M. Skibowski, “Charge-density-wave phase transition in 1T - TiSe₂: Excitonic insulator versus band-type Jahn-Teller mechanism,” *Phys. Rev. B* **65**, 235101 (2002).
- ⁴¹T. Pillo, J. Hayoz, H. Berger, and F. Lévy, “Photoemission of bands above the Fermi level: The excitonic insulator phase transition,” *Phys. Rev. B - Condens. Matter Mater. Phys.* **61**, 16213–16222 (2000).
- ⁴²H. Cercellier, C. Monney, F. Clerc, C. Battaglia, L. Despont, M. G. Garnier, H. Beck, P. Aebi, L. Patthey, H. Berger, and L. Forró, “Evidence for an Excitonic Insulator Phase in 1T - TiSe₂,” *Phys. Rev. Lett.* **99**, 146403 (2007).
- ⁴³C. Monney, H. Cercellier, F. Clerc, C. Battaglia, E. F. Schwier, C. Didiot, M. G. Garnier, H. Beck, P. Aebi, H. Berger, L. Forró, and L. Patthey, “Spontaneous exciton condensation in 1T - TiSe₂: BCS-like approach,” *Phys. Rev. B* **79**, 045116 (2009).
- ⁴⁴M. He, P. Rivera, D. Van Tuan, N. P. Wilson, M. Yang, T. Taniguchi, K. Watanabe, J. Yan, D. G. Mandrus, H. Yu, H. Dery, W. Yao, and X. Xu, “Valley Phonons and Exciton complexes in a Monolayer Semiconductor,” *Nat. Commun.* **11**, 618 (2020).
- ⁴⁵E. Liu, J. van Baren, C.-T. Liang, T. Taniguchi, K. Watanabe, N. M. Gabor, Y.-C. Chang, and C. H. Lui, “Multipath Optical Recombination of Intervalley Dark Excitons and Trions in Monolayer WSe₂,” *Phys. Rev. Lett.* **124**, 196802 (2020).
- ⁴⁶S. Brem, A. Ekman, D. Christiansen, F. Katsch, M. Selig, C. Robert, X. Marie, B. Urbaszek, A. Knorr, and E. Malic, “Phonon-Assisted Photoluminescence from Indirect Excitons in Monolayers of Transition-Metal Dichalcogenides,” *Nano Lett.* **20**, 2849–2856 (2020).
- ⁴⁷Z. Li, T. Wang, C. Jin, Z. Lu, Z. Lian, Y. Meng, M. Blei, S. Gao, T. Taniguchi, K. Watanabe, T. Ren, S. Tongay, L. Yang, D. Smirnov, T. Cao, and S.-F. Shi, “Emerging photoluminescence from the dark-exciton phonon replica in monolayer WSe₂,” *Nat. Commun.* **10**, 2469 (2019).
- ⁴⁸Z. Li, T. Wang, S. Miao, Y. Li, Z. Lu, C. Jin, Z. Lian, Y. Meng, M. Blei, T. Taniguchi, K. Watanabe, S. Tongay, W. Yao, D. Smirnov, C. Zhang, and S.-F. Shi, “Phonon-exciton Interactions in WSe₂ under a quantizing magnetic field,” *Nat. Commun.* **11**, 3104 (2020).
- ⁴⁹A. Castellanos-Gomez, M. Buscema, R. Molenaar, V. Singh, L. Janssen, H. S. J. van der Zant, and G. A. Steele, “Deterministic transfer of two-dimensional materials by all-dry viscoelastic stamping,” *2D Mater.* **1**, 011002 (2014).

- ⁵⁰M. R. Rosenberger, H. J. Chuang, K. M. McCreary, A. T. Hanbicki, S. V. Sivaram, and B. T. Jonker, “Nano-”Squeegee” for the Creation of Clean 2D Material Interfaces,” *ACS Appl. Mater. Interfaces* **10**, 10379–10387 (2018).
- ⁵¹O. A. Ajayi, J. V. Ardelean, G. D. Shepard, J. Wang, A. Antony, T. Taniguchi, K. Watanabe, T. F. Heinz, S. Strauf, X.-Y. Zhu, and J. C. Hone, “Approaching the Intrinsic Photoluminescence Linewidth in Transition Metal Dichalcogenide Monolayers,” *2D Mater.* **4**, 031011 (2017).
- ⁵²J. Wierzbowski, J. Klein, F. Sigger, C. Straubinger, M. Kremser, T. Taniguchi, K. Watanabe, U. Wurstbauer, A. W. Holleitner, M. Kaniber, K. Müller, and J. J. Finley, “Direct Exciton Emission from Atomically Thin Transition Metal Dichalcogenide Heterostructures near the Lifetime Limit,” *Sci. Rep.* **7**, 12383 (2017).
- ⁵³J. Jadczyk, J. Kutrowska-Girzycka, P. Kapuściński, Y. S. Huang, A. Wójs, and L. Bryja, “Probing of Free and Localized Excitons and Trions in Atomically Thin WSe₂, WS₂, MoSe₂ and MoS₂ in Photoluminescence and Reflectivity Experiments,” *Nanotechnology* **28**, 395702 (2017).
- ⁵⁴E. Liu, J. van Baren, Z. Lu, M. M. Altairy, T. Taniguchi, K. Watanabe, D. Smirnov, and C. H. Lui, “Gate Tunable Dark Trions in Monolayer WSe₂,” *Phys. Rev. Lett.* **123**, 027401 (2019).
- ⁵⁵C. Zhang, C. Gong, Y. Nie, K.-A. Min, C. Liang, Y. J. Oh, H. Zhang, W. Wang, S. Hong, L. Colombo, R. M. Wallace, and K. Cho, “Systematic study of electronic structure and band alignment of monolayer transition metal dichalcogenides in Van der Waals heterostructures,” *2D Mater.* **4**, 015026 (2016).
- ⁵⁶R. Sharma, J. Pandey, K. R. Sahoo, K. S. Rana, R. K. Biroju, W. Theis, A. Soni, and T. N. Narayanan, “Spectroscopic correlation of chalcogen defects in atomically thin MoS_{2(1-x)}Se_{2x} alloys,” *J. Phys. Mater.* **3**, 045001 (2020).
- ⁵⁷T. Verhagen, V. L. Guerra, G. Haider, M. Kalbac, and J. Vejpravova, “Towards the evaluation of defects in MoS₂ using cryogenic photoluminescence spectroscopy,” *Nanoscale* **12**, 3019–3028 (2020).
- ⁵⁸M. Tangi, M. K. Shakfa, P. Mishra, M.-Y. Li, M.-H. Chiu, T. K. Ng, L.-J. Li, and B. S. Ooi, “Anomalous photoluminescence thermal quenching of sandwiched single layer MoS₂,” *Opt. Mater. Express* **7**, 3697 (2017).

- ⁵⁹S. Tongay, J. Suh, C. Ataca, W. Fan, A. Luce, J. S. Kang, J. Liu, C. Ko, R. Raghunathan, J. Zhou, F. Ogletree, J. Li, J. C. Grossman, and J. Wu, “Defects activated photoluminescence in two-dimensional semiconductors: interplay between bound, charged and free excitons,” *Sci. Rep.* **3**, 2657 (2013).
- ⁶⁰K. Sugawara, Y. Nakata, R. Shimizu, P. Han, T. Hitosugi, T. Sato, and T. Takahashi, “Unconventional charge-density-wave transition in monolayer 1T-TiSe₂,” *ACS Nano* **10**, 1341–1345 (2016).
- ⁶¹F. J. Di Salvo, D. E. Moncton, and J. V. Waszczak, “Electronic properties and superlattice formation in the semimetal TiSe₂,” *Phys. Rev. B* **14**, 4321–4328 (1976).
- ⁶²P. Chen, Y.-H. Chan, X.-Y. Fang, S.-K. Mo, Z. Hussain, A.-V. Fedorov, M. Y. Chou, and T.-C. Chiang, “Hidden Order and Dimensional Crossover of the Charge Density Waves in TiSe₂,” *Sci. Rep.* **6**, 37910 (2016).
- ⁶³D. L. Duong, G. Ryu, A. Hoyer, C. Lin, M. Burghard, and K. Kern, “Raman Characterization of the Charge Density Wave Phase of 1T-TiSe₂: From Bulk to Atomically Thin Layers,” *ACS Nano* **11**, 1034–1040 (2017).
- ⁶⁴C. S. Snow, J. F. Karpus, S. L. Cooper, T. E. Kidd, and T. C. Chiang, “Quantum Melting of the Charge Density Wave State in 1T-TiSe₂,” *Phys. Rev. Lett.* **91**, 136402 (2003).
- ⁶⁵P. Tonndorf, R. Schmidt, P. Böttger, X. Zhang, J. Börner, A. Liebig, M. Albrecht, C. Kloc, O. Gordan, D. R. T. Zahn, S. Michaelis de Vasconcellos, and R. Bratschitsch, “Photoluminescence emission and Raman response of monolayer MoS₂, MoSe₂, and WSe₂,” *Opt. Express* **21**, 4908 (2013).
- ⁶⁶M. Balkanski, R. F. Wallis, and E. Haro, “Anharmonic effects in light scattering due to optical phonons in silicon,” *Phys. Rev. B* **28**, 1928–1934 (1983).
- ⁶⁷J. Joshi, I. R. Stone, R. Beams, S. Krylyuk, I. Kalish, A. V. Davydov, and P. M. Vora, “Phonon anharmonicity in bulk T_d-MoTe₂,” *Appl. Phys. Lett.* **109**, 031903 (2016).
- ⁶⁸L. Su, Y. Zhang, Y. Yu, and L. Cao, “Dependence of coupling of quasi 2-D MoS₂ with substrates on substrate types, probed by temperature dependent Raman scattering,” *Nanoscale* **6**, 4920–4927 (2014).
- ⁶⁹G. Grüner, *Density Waves in Solids* (CRC Press, 1994).
- ⁷⁰P. Wölfle, “Theory of sound propagation in pair-correlated Fermi liquids: Application to He 3 - B,” *Physical Review B* **14**, 89–113 (1976).

- ⁷¹K. F. Mak, C. Lee, J. Hone, J. Shan, and T. F. Heinz, “Atomically Thin MoS₂: A New Direct-Gap Semiconductor,” *Phys. Rev. Lett.* **105**, 136805 (2010).
- ⁷²S. Shree, I. Paradisanos, X. Marie, C. Robert, and B. Urbaszek, “Guide to optical spectroscopy of layered semiconductors,” *Nature Reviews Physics* **3**, 39–54 (2021).
- ⁷³T. Mueller and E. Malic, “Exciton physics and device application of two-dimensional transition metal dichalcogenide semiconductors,” *npj 2D Materials and Applications* **2**, 1–12 (2018).
- ⁷⁴T. Deilmann and K. S. Thygesen, “Finite-momentum exciton landscape in mono- and bilayer transition metal dichalcogenides,” *2D Mater.* **6**, 035003 (2019).
- ⁷⁵L. P. McDonnell, J. J. S. Viner, P. Rivera, X. Xu, and D. C. Smith, “Observation of intravalley phonon scattering of 2s excitons in MoSe₂ and WSe₂ monolayers,” *2D Materials* **7**, 045008 (2020).
- ⁷⁶C. Monney, E. F. Schwier, M. G. Garnier, N. Mariotti, C. Didiot, H. Beck, P. Aebi, H. Cerclier, J. Marcus, C. Battaglia, H. Berger, and A. N. Titov, “Temperature-dependent photoemission on 1T - TiSe₂: Interpretation within the exciton condensate phase model,” *Phys. Rev. B* **81**, 155104 (2010).
- ⁷⁷T. M. Project, “Materials data on MoSe₂ by materials project,” (2020), 10.17188/1191826.
- ⁷⁸H. Shibata, “Negative Thermal Quenching Curves in Photoluminescence of Solids,” *Jpn. J. Appl. Phys.* **37**, 550–553 (1998).
- ⁷⁹J. Huang, T. B. Hoang, and M. H. Mikkelsen, “Probing the Origin of Excitonic States in Monolayer WSe₂,” *Sci. Rep.* **6**, 22414 (2016).
- ⁸⁰S. S. Lin, B. G. Chen, W. Xiong, Y. Yang, H. P. He, and J. Luo, “Negative Thermal Quenching of Photoluminescence in Zinc Oxide Nanowire-Core/Graphene-Shell Complexes,” *Opt. Express* **20**, A706 (2012).
- ⁸¹A. Kogar *et al.*, “Signatures of exciton condensation in a transition metal dichalcogenide,” *Science* **358**, 1314–1317 (2017).
- ⁸²C. Lian, Z. A. Ali, and B. M. Wong, “Charge density wave hampers exciton condensation in 1T- TiSe₂,” *Phys. Rev. B* **100**, 205423 (2019).
- ⁸³D. Van Tuan, B. Scharf, I. Žutić, and H. Dery, “Marrying excitons and plasmons in monolayer transition-metal dichalcogenides,” *Phys. Rev. X* **7**, 041040 (2017).
- ⁸⁴D. Van Tuan, B. Scharf, Z. Wang, J. Shan, K. F. Mak, I. Žutić, and H. Dery, “Probing many-body interactions in monolayer transition-metal dichalcogenides,” *Phys. Rev. B* **99**,

085301 (2019).

⁸⁵B. Scharf, D. Van Tuan, I. Žutić, and H. Dery, “Dynamical screening in monolayer transition-metal dichalcogenides and its manifestations in the exciton spectrum,” *J. Phys. Condens. Matter* **31**, 203001 (2019).

⁸⁶D. Van Tuan, B. Scharf, I. Žutić, and H. Dery, “Intervalley plasmons in crystals,” arXiv:1901.02567 (2019).